Industrial Crops & Products 178 (2022) 114660

Contents lists available at ScienceDirect

Industrial Crops & Products

journal homepage: www.elsevier.com/locate/indcrop

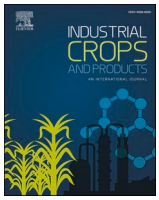

Isolation and characterisation of nanofibrillated cellulose from N36 *Ananas comosus* leaves via ball milling with green solvent

Surenthiran Gnanasekaran [a], Noor Ida Amalina Ahamad Nordin [a,*], Saidatul Shima Jamari [a], Jun Haslinda Shariffuddin [b]

[a] Faculty of Chemical and Process Engineering Technology, Universiti Malaysia Pahang, 26300 Gambang, Pahang, Malaysia
[b] College of Engineering, Chemical Engineering Department, Universiti Malaysia Pahang, 26300 Gambang, Pahang, Malaysia

ARTICLE INFO

Keywords:
Nanofibrillated cellulose
Ball-milling
Thermal stability
Crystallinity
Polydispersity
Isopropyl alcohol

ABSTRACT

The production of valuable materials from biomass into nanosized become the principal focus of the developing industries on achieving green-based composite product, designed for extensive range of applications. This study principally, focused on discovering green method for the utilisation of N36 *Ananas comosus* leaves fibre (PALF) to highly potential material. Nanofibrillated cellulose (NFC) were successfully isolated from PALF by ball milling with presence of isopropyl alcohol. The effect of isopropyl alcohol and the milling time on nano fibrillation were analysed through characterisation of NFCs including Field Emission Scanning electron microscopy (FESEM), X-ray diffraction (XRD), thermogravimetric analysis (TGA), Zeta-potential (ZP), Fourier transform infra-red (FTIR) and Particle size analysis (PSA). Comparatively, the 1:4—15 min NFC sample which milled for 15 mins with 1 mL of cellulose suspension and 4 mL of IPA, express desirable features in the concern of morphology, fibre size, yield, crystallinity, thermal stability, and homogeneity on disintegration of PALF fibre. High thermal degradation temperature of 323 ℃ and crystallinity index of 67%, reveal the potential on reinforcing to improve the composite's thermal stability and mechanical properties. Moreover, it exhibits excellent surface morphology, stability with low self-agglomeration, and uniformity in defibrillation with fibre diameter of 25.84 ± 8.30 nm, zeta-potential of − 32.31 ± 2.51 and PDI of 0.103. Besides, the high yield of NFC (>90%), increase the feasibility of NFC production. Hence, addition of IPA gives significant impact on defibrillation by disrupt the intermolecular hydrogen bond, so that less milling time is convenient on production of NFC without causes severe damage on other properties.

1. Introduction

Cellulose is the most abundant and available biopolymer on earth, consisting of complex carbohydrate molecules made up of linear glucose units linked together by β− 1,4-glycosidic linkages with repeating units at different degree of polymerisation (Nuruddin et al., 2016). The occurrence of hydroxyl groups, carried by these individual monomer units, facilitate formation of inter and intra molecular hydrogen bonds and packed into microfibrils bundle, which offer well-ordered three--dimensional crystalline structure to control the physical characteristics. The proper deployment of these cellulose stimulates promising sustainable growth of green composite (Galiwango et al., 2019). The nanocellulose isolation from agricultural biomass has received substantial progress in recent times while several products been commercialised and currently available. In order to claim as nanocellulose, at least one dimension of physical aspect should be less than 100 nm. Nanofibrillated cellulose (NFC), nanocrystalline cellulose (NCC) and bacterial cellulose are the main three category of nanocellulose (Wu et al., 2021). NFC has a specific position as a class of low-cost, biodegradable, and potentially recyclable high-strength polymeric fibrils derived from renewable resources (Yang et al., 2020a, 2020b). NFC is frequently isolated from waste materials generated in connection with the production of agricultural products, for instance peel, leaves, stem and branch.

Pineapple (*Ananas comosus*) are mostly cultivated in tropical and subtropical countries and the post harvesting substantially have greater ratio of waste than the temperate fruits (Todkar and Patil, 2019). The global production of pineapple in 2018 is about 27.92 million metrics tons, and currently almost 1022,319 Ha area being utilised on pineapple plantation (Pereira et al., 2021; Najeeb et al., 2020). Malaysia has been

* Corresponding author.
E-mail address: idamalina@ump.edu.my (N.I.A. Ahamad Nordin).

https://doi.org/10.1016/j.indcrop.2022.114660
Received 9 August 2021; Received in revised form 13 January 2022; Accepted 5 February 2022
Available online 15 February 2022

recorded in the top 20 country which own an area of 10,847 ha with an estimated annual fruit production of 272,570 metric ton (Gnanasekaran et al., 2020b). Sarawak, Josaphine, Moris, Gandul, N36 and MD2 are the common pineapple cultivars in Malaysia (Jaji et al., 2018). As reported by Lee et. al, (2020), approximately 15 tonnes of PALF are generating as waste from one hectare of pineapple plantation by annually (Lee et al., 2020). This statistic eventually indicating the abundancy and availability of pineapple biomass to comply with the demand of bio-composite manufacturers and Malaysia's research and development department. In that concern, PALF own distinctive combination of properties for instance, high strength, stiffness, and low density that make it an ideal source for nanofibre production. Moreover, the higher cellulose content in PALF than OPEFB (Mahadi et al., 2015), pine (Baruah et al., 2018) and corn stover (Kian et al., 2019) were reported. Prado and Spinace (2019) postulated that PALF owns 81.27% cellulose, 12.31% hemicellulose, 3.46% lignin and 10.52% moisture content (Prado and Spinacé, 2019). Evidently, the low content of lignin increases the feasibility on isolation of NFC with minimal downstream product.

Various method been recommended on production of nanocellulose, but mechanical treatments are the typical method such as grinding (Okahisa et al., 2011), ultrasonication (Kayes Patoary et al., 2020), refining (Hu et al., 2017), high pressure homogenisation (HPH) (Pakutsah and Aht-Ong, 2020), microfluidization (Sun et al., 2018) and ball milling (Ling et al., 2019). High shear force with operation of these pre-treatments, ensuing the fibrillation by facilitating the cleavage of cellulose fibre. However, high energy consumption and heterogeneity in fibrillation still become the limiting factor on implementation of these method. Other than that, clogging the small slit in the HPH due to fibre agglomeration could cause severe damage on the instrument (Zhang et al., 2015). To remedy this, the combinations of enzymatic or chemicals pre-treatments are currently being intended to facilitate mechanical pre-treatments by removing the non-cellulosic materials and enriching cellulose accessibility. For example, numerous chemical treatments, such as TEMPO-oxidation (Boufi and Chaker, 2016), carboxylation, sulphonation (Rashid and Dutta, 2020), phosphorylation (Noguchi et al., 2017), esterification (Ahuja et al., 2021) have been successfully achieved this target, but the use of hazardous reagent, corrosion, difficulty in chemical recovery and process efficiency, limits the feasibility of treatments (Cebreiros et al., 2021).

Ball milling is another mechanical treatment where, the rotation of vessel creates the centrifugal force and induce high shear forces among balls and ball with surface of vessels. These high intense force causes the cracking of cellulose fibrils into smaller size. Presently, ball milling is extensively utilised for the production of NFC owing to its uncomplicated operation, economical equipment and applicable to majority of biomass. The ambient condition as operating parameter is another advantage over other mechanical treatments (Sofla et al., 2016). In addition, the basis (wet or dry), type of ball, size of ball, milling time, type of solvent, angular velocity of milling jar, solid content (Sc), ball to fibre mass ratio (BMR), are significant factors to be considered during ball milling. The selection and composition of solvent play vital role on nanofibrillation. In previous study Nagarajan et al. (2019) used deionized water as solvent on nanofibrillation of *Cocos nucifera var Aurantiaca* and obtained cellulose fibrils with diameter of 9–15 μm, while Nuruddin et al. (2016) applied 80% of ethanol/water mixture for nanofibrillation of kenaf fibres and wheat straw and achieved cellulose nanofibrils with diameter of 8–100 nm. As reported utilisation of alcohol gives significant impact on nanofibrillation and make the process more feasible. Besides, Jahangiri et al. (2016) has reported that particles which milled in isopropyl alcohol (IPA) have the smaller size and lowest density than the ones milled in ethanol. Thus, IPA has been selected as solvent for this study. Currently, there is limited available information in the literature regarding, relationship of solvent other than ethanol and milling time on isolation of NFC, especially from PALF.

In this study, chemo-mechanical paired treatment was developed on isolation of NFC from N36 cultivar PALF by ball milling with presence of IPA as green solvent. The hypothesis of this study is the increments in IPA reduce the intermolecular hydrogen bond and act as co-surfactant by facilitating the homogenous defibrillation of cellulose fibre with low milling time. FESEM, FTIR, XRD, TGA have been completed in order to characterise the morphology, surface functional groups, crystallinity, and thermal stability of obtained NFCs, respectively. The gravimetrical yields, zeta potential, optical transmittance, particle size analyses of NFCs were also considered to evaluate the properties of NFCs.

2. Methodology

Raw material which is, N36 *Ananas comosus* leaves (PALF) were gathered from Pekan Pina Sdn. Bhd plantation, Pahang, Malaysia. Sodium hydroxide (NaOH), sodium chlorite ($NaClO_2$) and acetic acid (98%), analytical grade (CH_3COOH), were purchased from Sigma Aldrich, Germany. While Isopropyl alcohol, ($(CH_3)_2CHOH$) was purchased from Merck, Germany.

2.1. Preparation of cellulose

Cleaned and dried leaves were crushed using SCV7510 TST Plastic crusher with 1 mm gap opening. PALF fibre were treated with steam-alkaline coupled treatment (SAC) at temperature of 121 °C and pressure of 21 psia with 1.0 wt% of NaOH for 1 h using Hirayama HVE-50 Autoclave Steriliser (Gnanasekaran et al., 2021a). SAC treated fibre was bleached with 3 wt% of $NaClO_2$ for 90 min at temperature of 70 ℃ while 1:50 was fixed as SAC fibre to $NaClO_2$ solution. Aliquot drops of glacial acetic acid were added until attain a pH of 4.5–4.8 to establish acidic condition (Gnanasekaran et al., 2021b). Cellulose fibres were washed with distilled water after the bleaching treatment and proceed to NFC production.

2.2. Production of nanofibrillated cellulose (NFC)

Initially, 1 wt% of cellulose suspension were prepared in distilled water and left for 48 h for hydration (Guimaraes et al., 2015). One mL cellulose suspension (1 wt%) were mixed with different volume of IPA (3 and 4 mL) and milled in Fritsch Pulverisette 7 planetary ball milling system with 2 grinding station using 1 mm diameter of zirconia ball. The milling vessel was filled with ball to cellulose fraction of 70:1 and milled at angular rotational speed of 700 rpm at atmospheric pressure and room temperature of 25 ℃ (Nagarajan et al., 2019). The milling time was varied into 15 and 30 min. Table 1 represented the designation of experiment and denotation of NFC sample. Fig. 1 illustrated the overall process flow on NFC production.

2.3. Characterisation of NFC

The NFC samples were freeze-dried from an aliquot NFC suspension obtained from ball milling for long term storage. The NFC suspensions were frozen at − 80 ℃ for 24 h prior to lyophilise process. The frozen NFC sample were placed in freeze dryer chamber (BenchTop Pro with Omnitronic™, SP Scientific) and freeze dried on auto mode at pressure

Table 1
Designation of experiment and denotation of NFC sample.

Sample	Volume of cellulose suspension, mL	Volume of IPA, mL	Solid content, wt%	Time, min
1:3—15 min	1	3	0.30	15
1:3—30 min	1	3	0.30	30
1:4—15 min	1	4	0.25	15
1:4—30 min	1	4	0.25	30

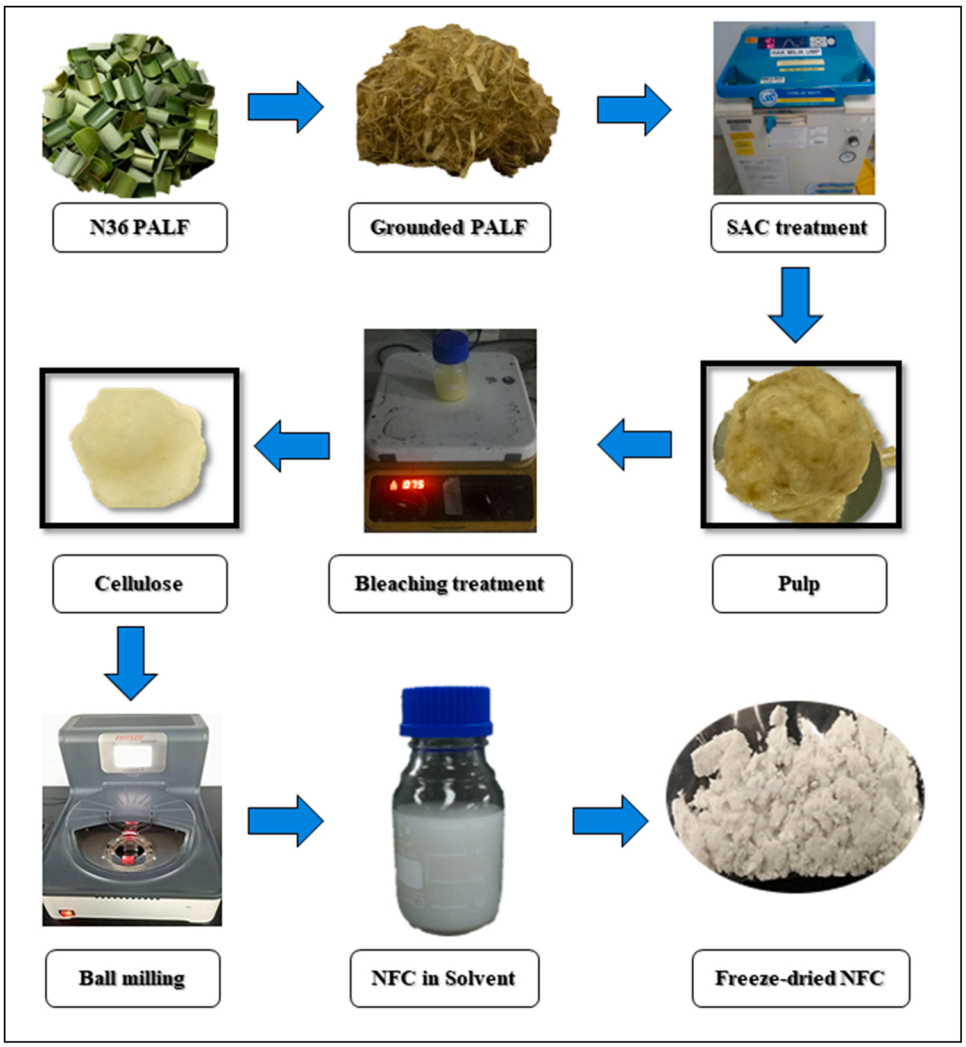

Fig. 1. Summary of overall experimental process flow.

of 50 mT and temperature of − 90 to − 97 ℃ for 48 h. The freeze died specimens were used for characterisation of NFC. The remaining samples were stored in desiccator till further use.

2.3.1. Physical appearance of NFC

Priorly, the NFC samples were placed in 50 mL of Scott bottle and sonicated for 15 min to achieve uniform distribution in IPA. Then, the physical appearance of NFC suspension was captured.

2.3.2. Yield in nanofibrillated cellulose

NFCs suspension with solid content (Sc) of 0.1% were centrifuged for 15 min at 4000 rpm to split the nanofibrillated NFC from the non-fibrillated or partially fibrillated NFC that settled at the bottom. The sediment portion was dried at 90 ℃ until constant weight obtained. The yield of NFCs was computed using equation Eq.1 (Kayes Patoary et al., 2020):

$$Yield(\%) = \left(1 - \frac{weight\ of\ dried\ sediment}{weight\ of\ diluted\ sample \times \%Sc}\right) \times 100 \quad (1)$$

2.3.3. Optical transmittance and visual examination of NFC

The light transmittance of 0.1% w/v NFC suspensions was assessed in the range of 800–300 nm by using Hitachi (U-1800) UV–Vis spectrophotometer in quartz cuvettes. Water-filled cuvette was used as blank (Cebreiros et al., 2021).

2.3.4. FTIR of NFC

The FTIR spectra were recorded on a Spectrum 400 FT-IR spectrometer using Thermo Scientific Nicolet iS5. The NFC suspension were lyophilised to shape sample into powder form. The samples were placed on top of the steel plate and measured the spectral at range of 500–4000 cm^{-1} at the resolution of 4 cm^{-1} directly and the average scans were taken for every sample (Sartika et al., 2021).

2.3.5. X-ray diffraction (XRD) of NFC

The diffractograms of prepared NFC were determined from X-ray attained with Rigaku Mini Flex II equipped with a CuKα radiation λ = 0.154 mm at 30 kV and 15 mA. The scattered radiation in the range of 2θ from 5° to 40° were recorded and the data acquisition taken at intervals of 0.05° for 2 s. The crystallinity index (CrI) value for the NFC were calculated according to equation Eq.2:

$$\mathrm{CrI}(\%) = \left(\frac{I_{200} - I_{am}}{I_{200}}\right) \times 100 \quad (2)$$

where I_{200} is corresponds to the intensity of the main peak at (200) lattice and I_{am} denotes the peak intensity at amorphous region with minimum diffraction intensity (Santucci et al., 2016).

2.3.6. Thermogravimetric analysis (TGA) of NFC

Thermal stability of NFC samples was tested with aid of Hitachi STA7200 Thermal Analysis Instrument (TGA-Q500) with ramping

temperatures from 30 °C to 600 °C under a nitrogen gas with a flow rate of 100 mL/min and a heating rate of 10 °C/min. Approximately 3 – 4 mg of the specimen was intended for TGA test. Acquired the derivative forms of DTG by differentials of TGA using the central finite difference approach as follows Eq.3 (Seta et al., 2020).

$$DTG = \frac{W_{t+\Delta t} - W_{t-\Delta t}}{2\Delta t} \quad (3)$$

Where $W_{t+\Delta t} - W_{t-\Delta t}$ are the residual weight of the sample at time $t + \Delta t$ and $t - \Delta t$, respectively, and Δt is the time interval for reading residual sample weight.

2.3.7. Field emission scanning electron microscopy (FESEM)

About 0.003 g of freeze dried of each NFC samples were re-suspended in 30 mL of distilled water (0.01% w/v) and sonicated for 15 min to achieve uniform distribution (Beyene et al., 2018). At room temperature, a drop of nanosuspension were deposited onto ultra-thin conductive carbon tape and dried. The morphology of dried NFCs sample was analysed by a field emission scanning electron microscope (FE-SEM) using JEOL JSM 7800 F with a resolution acceleration of 5–15 kV (0.5 nm at 1 kV). Prior to analysis the samples were platinum sputtered-coated using JEOL JFC-1600 Auto Fine Coater at 5 kV to compromise the image charging. Using Image J software, the NFC fibre size was calculated based on the average diameter of 100 random fibres (Supian et al., 2020).

2.3.8. Zeta potential, ξ

The NFCs were diluted to a concentration of 0.01 wt%. The zeta potential of aqueous NFC suspension was determined using DelsaMax Pro (3234-DMP, Beckman Coulter) to evaluate electrophoretic mobility of particles and converted to Zeta potential (ξ) using Eq.4. 10 s has been set up as reading time to record the zeta potential data, and the measurements were done in triplicate using the final mean values. (Ferreira et al., 2020).

$$\xi = \frac{3\eta U_E}{2\varepsilon f(ka)} \quad (4)$$

Where, η is corresponds to viscosity, U_E for electrophoretic mobility, ε for dielectric constant and $f(ka)$ stands for Henry's function.

2.3.9. Particle size measurement by DLS analysis

Intensity-weighed mean (z-average diameter), and polydispersity index (PDI) of NFCs were determined by Dynamic Light Scattering (DLS) analysis using Zetasizer nano series (Nano-S90, Malvern Instruments, UK) by having a He-Ne laser of wavelength 633 nm at 25 ℃, and a backscatter detector (173°). To obtain the statistical distribution of particle size by DLS, 0.01% (w/v) of NFCs were re-suspended in deionized water and sonicated for 15 min to achieve uniform distribution (Sai Prasanna and Mitra, 2020). All measurements for each sample were performed in triplicate.

2.3.10. Moisture analysis

A&D's MS-70 Moisture Analyser was used to determine the moisture content. Placed 0.15 – 0.20 g of NFC on aluminium pan and run the analysis at temperature of 105 ℃. Recorded the result of moisture content of the sample after the programme end.

3. Results and discussion

3.1. Physical appearance of milled NFC

Fig. 2 show the physical changes and appearance of NFCs sample after milled at designed milling time and volume of IPA as shown in Table 1. Based on Fig. 2, the colour of 1:4—15 min NFC suspension is comparatively less dark than other NFCs suspension due to degradation of cellulose materials, on PALF nanofibre which may lead to formation of high amount of residue (Hu et al., 2017). Conferring to Wang et al. (2021), the dark colour of NFC suspension may attributed to the factor of carbonisation of cellulosic fibrils. This trend is commonly occur due to fibre damage during ball milling with strong mechanical force (Xie et al., 2018). Although, ball milling time is the essential parameter on defibrillation of microfibre bundle into nano size, but the increasing of milling time resulted in higher amount of contamination from the wall of container and possibly from milling balls in the NFC suspension. However, using optimised milling time with aid of solvent as surfactant may effectively reduce the contamination (Amiralian et al., 2015).

3.2. Optical transmittance of NFCs suspension

UV–vis spectroscopy has been conducted to obtain evidence on the impacts of solvent and milling time on the transparency of the NFC suspensions. The intensity of transparency also reflects the size of the fibres (Goh et al., 2016). The transmittance curve from 300 to 800 nm is a simple mean to get an approximate idea about the change in the fibrillation yield and the dispersibility of the cellulose nanofibrils in water (Boufi and Chaker, 2016). As witnessed from the UV-Vis spectra shown in Fig. 3, 1:4—15 min and 1:4—30 min sample have the maximum and similar optical transmittance followed by 1:3—30 min and 1:3—15 min fibres. Furthermore, the transmittance is firmly dependent on the wavelength; it declines with decreasing wavelength (Yang et al., 2020a, 2020b). The light will scatter when it passes through a nanocellulose suspension holding randomly dispersed particles due to the fact that the scattering occurs when discontinuation in the refractive index happens, ultimately causing a decrease in the transparency degree (Nurul Atiqah et al., 2019). Therefore, increasing of IPA volume significantly increase the defibrillation of NFC, by rise on the transparency of suspension. These phenomena proved that effective nano fibrillation occurred at 1:4—30 min and 1:4—15 min

3.3. Gravimetrical yield of NFCs

Essentially, an heterogeneous materials, such as fibre, fibre

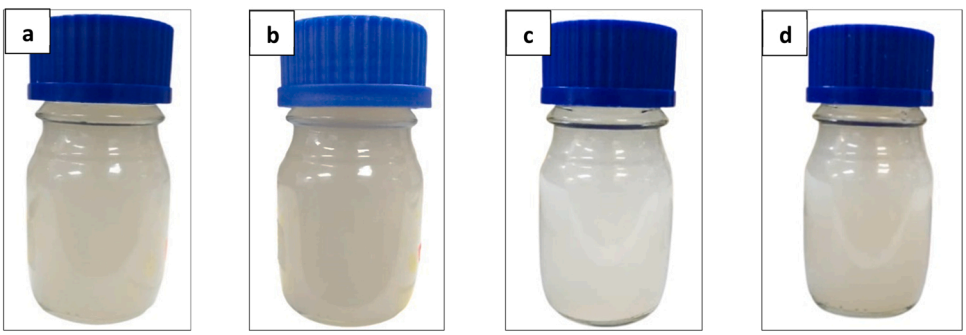

Fig. 2. Physical appearance of (a) 1:3— 15 min, (b) 1:3—30 min, (c) 1:4—15 min, (d) 1:4—30 min NFCs after ball milled.

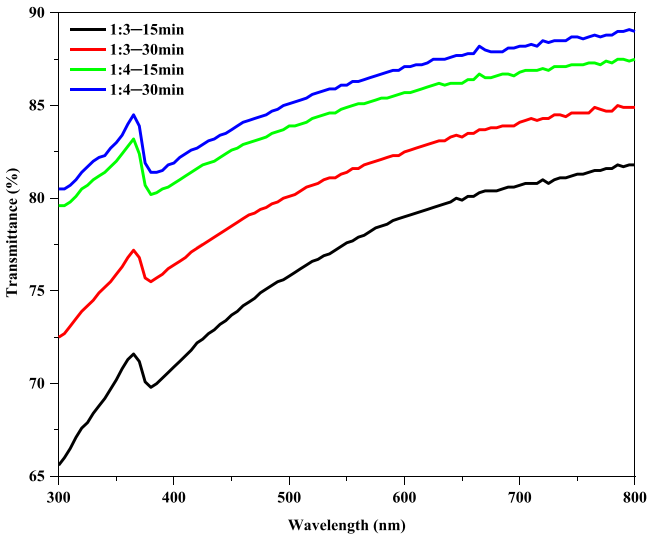

Fig. 3. Optical transmittance of NFCs suspension at 300–800 wavelength.

fragments, fines and fibrils are the common on mechanical fibrillation (Fillat et al., 2018). Thus, the gravimetric yields or yields of individual nanofibre cellulose were consequently computed based on the fraction of the NFC concentration in the supernatant fluid after centrifugation to a solid concentration before centrifugation (Noguchi et al., 2017). As observed from Fig. 4, the yield of 1:4—30 min is (94.39 ± 0.94), which is higher than 1:4—15 min (92.45 ± 0.92), 1:3—30 min (91.89 ± 0.92) and 1:3—15 min (90.85 ± 0.91). The obtained yield are nearly similar with Phanthong et al. (2017) who successfully obtained 93.1% yield of NFC extracted from cellulose powder by using planetary ball milling in the presence of ionic liquid. Increment in milling time increase the collision of incident with ball and NFC suspension in milling vessel. Therefore, the intermolecular hydrogen bond (—H) of fibre, efficiently broken up and increase the degree of defibrillation significantly (Dilamian and Noroozi, 2019). However, the yield of 1:4—15 min approximately similar with 1:3—30 min, consequently increasing the volume of IPA play a crucial role in weakening the hydrogen bond to reduce surface energy of microfibrils as well. Reducing in surface energy, demands less kinetic energy to disintegrate the fibrils. Thus, energy consumption also has to be considered on yield of nanofibers to prevent excessive energy usage (Liu et al., 2019).

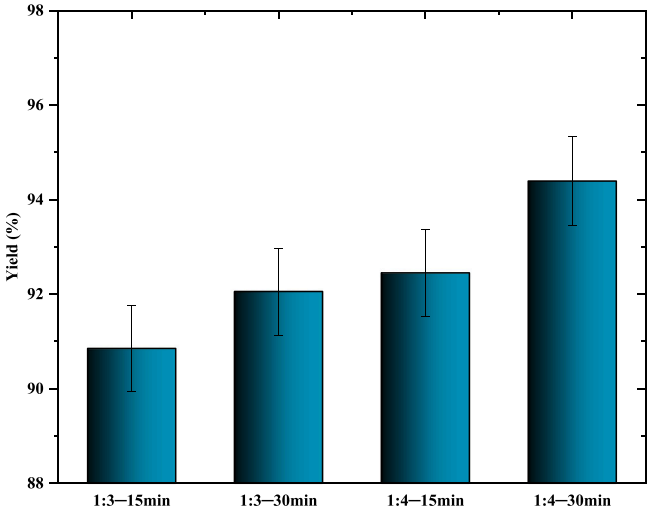

Fig. 4. The percentage of NFC yield after ball milling.

3.4. Fourier transform infra-red (FTIR) spectroscopy of NFCs

Fig. 5 illustrated the FTIR spectra results of NFCs to observe the changes in chemical bond or functional group after the nano fibrillation of cellulose. Commonly, the cellular wall of the PALF possess insoluble polysaccharides that constituted of cellulose, hemicellulose and pectin (Mat Zain, 2014). Moreover, alkanes, alcohol, aromatic, and ester were the main functional group for these lignocellulosic fibre components. The peaks at 1240 and 1499 cm^{-1} found in the spectrum, correspond to the aromatic skeletal vibrations of remaining lignin. Observed the band at 1734 cm^{-1} is attributed to the stretching vibration of the uronic ester and acetyl groups (C═O) in pectin, hemicelluloses, or the ester linkage of carboxylic group of ferulic and p-coumaric acids of lignin and/or hemicelluloses (Akinjokun et al., 2021). The sharp peak which appeared at 1150 and 1085 cm^{-1} represent the stretching vibration of the pyranose ring skeletal (C—O—C) link between polysaccharides unit in cellulose. In addition, the substantial intense peak at 986 cm^{-1} and a shoulder peak in the region of 890 cm^{-1} correspond to the (—C—H) glycosidic deformation of cellulose component. Moreover, the crystalline band of cellulose indicated by two sharp peaks at 1426 and 890 cm^{-1} (Julie Chandra et al., 2016). The wide absorption band around 3330 cm^{-1} equivalent to the stretching vibration of hydroxyl group (—OH), signalling hydrophilic properties of NFCs sample, while the weak band at 2910 cm^{-1} attributed to asymmetric CH_2 stretching (Gabriel et al., 2021). Relatively, ball-milling disintegration of cellulose did not lead to main change on FTIR spectrum. It proved that the mechanical treatment majorly causes changes in physical properties without change the chemical properties of NFCs sample. However, the absorption peak imputed to the —OH stretching vibrations become broader on NFC 1:4—15 min and 1:4—30 min, implying that, in accordance with the mechanical activation, the intermolecular hydrogen linkage of cellulose was subsided, and the quantity of free hydroxyls subsequently increased (Hu et al., 2017).

3.5. FESEM

Morphological and structural characterisation of ball-milled NFCs were analysed using FESEM. Natural fibre is a composite material, primarily composed of cellulose which act as main reinforcement. Additional components like lignin and pectin work as cementing materials to make fibril bundles. The removal of these binding materials helps to increase the accessibility of nanocellulose using mild thermal-chemical treatment. Fig. 6 shows topography of NFC after ball-milled with 15 and 30 min with different concentration of IPA parallel with lognormal distribution of fibre diameter. Fig. 6 show the shape and size of NFC produced using ball milling. Highly web like entangled cellulose

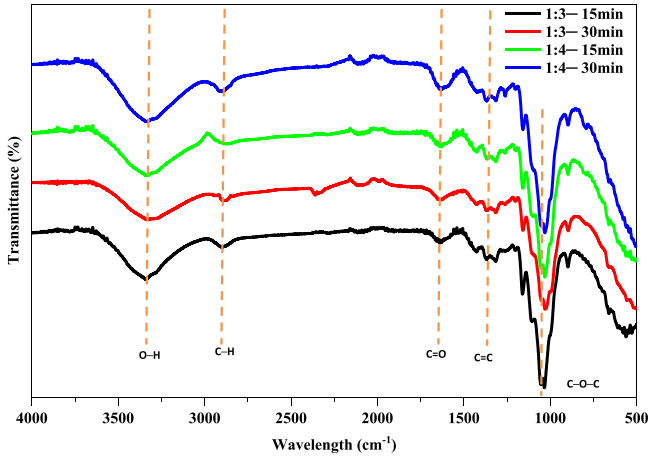

Fig. 5. FTIR spectra of ball-milled NFCs sample.

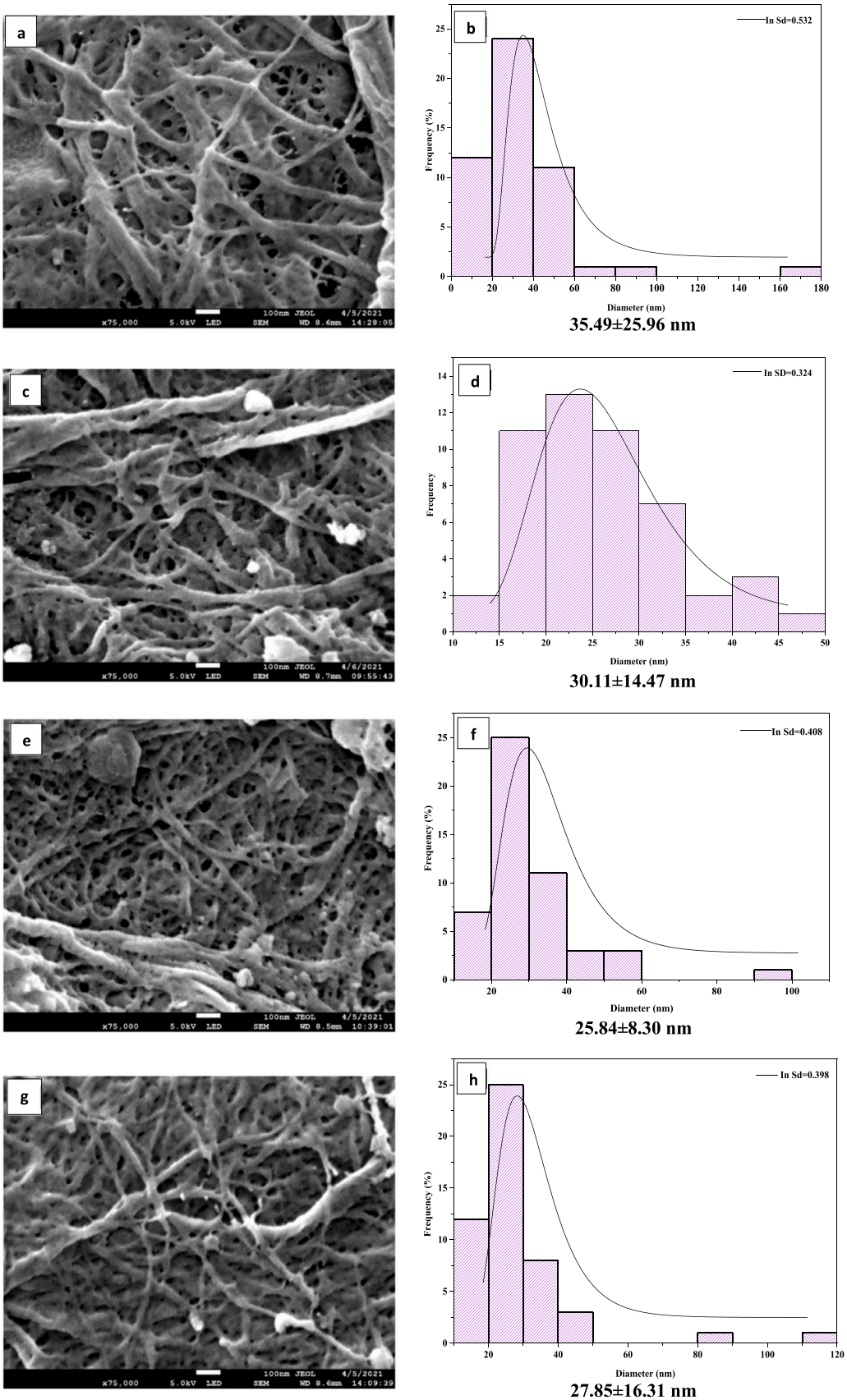

Fig. 6. FESEM micrography of (a) 1:3—15 min, (c) 1:3—30 min, (e) 1:4—15 min, (g) 1:4—30 min NFC at × 75,000 magnification and (b), (d), (f), (h) are the lognormal fibre size distribution of respective NFC.

nanofibre proved the drastic reduction of fibre size with aid of mechanical treatment. All the sample may claim as NFC since the diameter of fibre is below than 100 nm. Basically, crystalline sections are more robust to mechanical force which formed during ball milling compared with amorphous region of cellulose. Among the samples, 1:4—15 min and 1:4—30 min NFCs diameter distributions are more convenient in fibre size reduction than other samples. The longer milling time offer higher number of collision events between ball and fibre, which leads to a greater chance for breakdown of hydrogen linkage between cellulose fibrils to isolate the nano fibre. However, the ball-milling significantly, degrade the PALF nanofibre which corresponding to darker physical appearance as shown in Fig. 2. Ball milling treatment for 30 min split open the fibre into irregular small fragment which tend to form clump, but the longitudinal fragmentation was dominant as view in Fig. 6(c) and (g). The aggregation of these irregular fragment showing the higher degree of destruction of the PALF nanofibre. Mazela et al. (2020) also have experienced the same observation on degradation of nanofibrillated Södra Black R cellulose as increased the time of mechanical treatment. Remarkably, the increasing in volume of IPA as solvent enabled intra-fibril swelling of cellulose and weaken the hydrogen bonding between fibril bundles and make the mechanism of defibrillation of cellulose more feasible with minimal consumption of milling time. Moreover, the swelling tendency on cellulose may leading to less aggregation and homogenous distribution while ball milling and increase the effectiveness of ball-to-fibre collision impact too. Therefore, NFC that milled with high volume of IPA express better nano fibrillation with great reduction in fibre diameter of 25.84 ± 8.30 nm and low standard deviation, which indicating better homogeneity of nanofibril (Mazela et al., 2020). As mentioned by Han et al. (2019) the dispersion reveals that hydrogen bonding between nanofibers is lower. Hence, IPA stimulate better fibre defibrillation in content of, high homogeneity, less irregular fragments, low degradation of crystalline region and energy conservative.

3.6. Zeta potential and particle size analysis of NFC

The Zeta potential (ζ) is derived from the measurement of the nanoparticle mobility distribution after employed to an electric field and it applied to assess the surface charge of nanofibre. The surface charge is the key factor for determining the stability of the nanofibrillated cellulose suspension in water (Rashid and Dutta, 2020). The NFCs had a mean zeta potential reading at range of − 25.62 ± 4.29 mV to − 30.8 ± 0.5 mV as presented in Table 2. The negative ZP values are owing to the existence of hydroxyl groups (Ferreira et al., 2020; Franco et al., 2019).

Based on Table 2, all the NFCs sample are considered stable with absolute value greater than − 25 mV. However, 1:4—15 min and 1:4—30 min nanocellulose are comparatively more stable than other NFCs due to having higher value of zeta potential (Mazela et al., 2020). This trend occurred because high volume of IPA acts as a better co-surfactant by reducing the surface tension of cellulose fibre during ball milling, leading the effective collision impact on amorphous region of cellulose chain which subsequently increase the abundancy of hydroxyl group. These negatively charged hydroxyl group (—OH) trigger the electrostatic repulsion between the nanocellulose particle. Additionally, these electrostatic repulsion force stimulate well distribution of nanocellulose with less self-aggregation as shown in FESEM morphology (Czaikoski et al., 2020). Conversely, the z-average of 1:3—15 min and 1:3—30 min obtained by DLS analysis to be 105.50 nm and 96.54 nm respectively as stated in Table 2. This result, slightly contrast with the diameter distribution of nanofibre which measured from FESEM topography due to instability of nanofibre to form less repulsive force caused by limited amount of free hydroxyl group. It probably instigated to the self-aggregation and flocculation which ultimately commanded to sedimentation under gravitational force gravity to form larger fibre sizes during DLS analysis as shown in Fig. 7 (Sai Prasanna and Mitra, 2020). These facts are coherent with high PDI value of 0.950 and 0.832, which inferring heterogeneity of particle size and agglomeration in suspension (Wu et al., 2021). Sofla et al. (2016) suggested the formation of a fibrous layer or coating on the milling ball reduced the effectiveness of the impact force of the balls on the PALF fibre which implying non-uniformity of particle size by increasing PDI value. This is the main reason for increasing in PDI value of 1:4—30 min, even if increase the volumes of solvent. Therefore, increasing in milling time, would not provide significant impact on uniform defibrillation.

Table 2
Z-average, polydispersity (PDI) and zeta potential of nanofibre cellulose suspension.

NFCs	Z-average (nm)	PDI	Zeta potential, ξ (mV)
1:3—15 min	105.50	0.950	-25.62 ± 4.29
1:3—30 min	96.64	0.832	-25.08 ± 2.58
1:4—15 min	75.82	0.103	-32.31 ± 2.51
1:4—30 min	83.73	0.304	-30.72 ± 5.96

3.7. XRD analysis

X-ray diffractograms of milled nanofibrillated cellulose are exhibited in Fig. 8 to investigate the influence of increasing the volume of IPA as solvent and the milling time on the crystallinity. The diffractograms shows two main peaks around 2θ of 22—23° with a crystalline plane (200) which contribute to crystalline fraction, 15.5°—16° with a crystalline plane (110), which contribute to amorphous fraction of NFCs. The height of peak exposes the intensity of crystalline and amorphous region present in tested NFCs. According to the literature, the above mentioned crystallographic planes verify that the NFC samples are in the crystal structure and attributed to standard structure of cellulose I polymorph (Radakisnin et al., 2020). Apparently, the diffractogram of 1:4—15 min shows highest peak around 2θ= 23° due to high accessibility of crystalline region caused by disintegration of micro fibre bundle into nanofibrils. These trend consequently, lead to releasing of hydroxyl group which evident the presence of shoulder at amorphous region (Ilyas et al., 2019). Removing of amorphous region increase the hydroxyl group in suspension. During freeze-drying process, the ice crystals were formed by sublimation, the interfibrillar hydrogen bonding between the high number of hydroxyls on the surface of nanofibre cellulose self-assembles in an organised manner and resulted in increased crystallinity (Shahi et al., 2020). Cellulose nanofibers with greater crystallinity offer enhanced rigidity and stiffness which an effective property for the reinforcement of composite materials in order to improve the mechanical properties (Dilamian and Noroozi, 2019).

As specified in Table 3 the crystallinity index of 1:4—15 min which is 66.59% comparatively higher than other NFCs sample and in agreement with other study on extraction of NFC from pineapple leave fibre (Ling et al., 2019). Less crystallinity of the other NFCs are justified by the inefficient break resulting in the impact and shear forces or to the excessive time that resulted in the breaking of both the amorphous and crystalline regions (Ferreira et al., 2020). The increments in volume of IPA leads intra-fibril swelling and facilitate better defibrillation of the fibre bundle into nanofibril gradually and it may an alternative to use low times in the ball mill and guarantee the aimed properties in the dimensional and stability characteristics of the nanocellulose (Amiralian et al., 2015). However, increasing of milling time showed slight declining in the crystallinity index of NFC due to fractional damage on crystalline structure (Nagarajan et al., 2019).

These similar outcomes reported by Zheng et al. (2018) that ball milling interrupted the ordered crystalline structure of cellulose and the amorphization of cellulose continued with milling time, prominent to a continuous reduction in tensile strength of cellulose crystallites. Even though, extended milling time induce further fibre diameter reduction, the worsening of crystallinity index remains an uncompromising

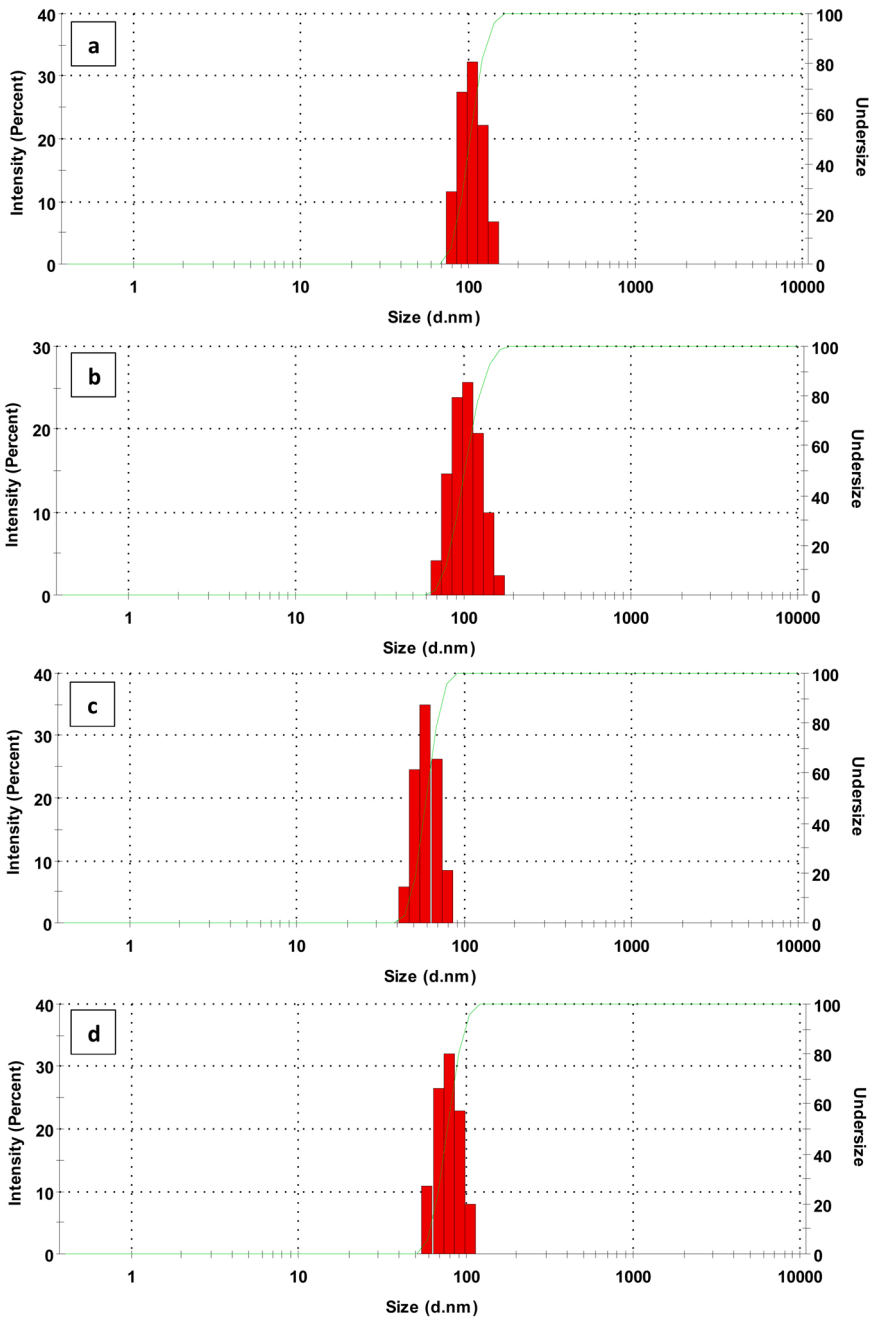

Fig. 7. The intensity of particle size distribution of (a) 1:3—15 min, (b) 1:3—30 min, (c) 1:4—15 min, (d) 1:4—30 min NFCs by DLS.

element in reinforcing sector and give a major drawback on thermal stability.

3.8. Thermal stability and moisture content of NFC

Thermogravimetric analysis was employed to inspect the thermal stability of the ball-milled NFCs. Determination of the thermal properties of nanofibre cellulose as reinforcing is critical to evaluate the applicability and compatibility these materials in bio-composite applications at high temperatures (Saurabh et al., 2016). The thermogram (TG) and derivative thermogram (DTG) curve were plotted in Fig. 9(a) and (b) respectively to track the thermal stability deviations of PALF nanofibre samples. Eventually, the DTG curve permitted for more specific appraisal and comparison (Goh et al., 2016). The maximum thermal degradation temperature (T_{max}), moisture content (MS), onset temperature (T_{on}), offset temperature (T_{off})) and residue or char content at 700 ℃ were summarised in Table 4. As it can be seen in Fig. 9(a) all the PALF nanofibre shows two weight loss stage.

The weight loss from room temperature to 105 ℃ is considered as the removal of physically bonded water or free water by evaporation which associate with moisture content of nanofibre cellulose (Sun et al., 2016; Ismail et al., 2021). These moisture content, express the hydrophilicity of ball-milled NFCs. According to Table 4, moisture content of 1:4—15 min remarkably higher than the other NFCs due to the abundancy of free —OH group which promote water absorption (Gnanasekaran et al., 2020a). The high surface area caused by defibrillation of fibre also one of main reason for moisture absorption as well (Gea et al., 2020). The presence of these high hydroxyl group was confirmed at X-ray diffractogram, previously. The second stage of thermal degradation took place approximately around 260 ℃ (T_{on}) to 330 ℃ (T_{off}) caused by thermal decomposition of hemicellulose and cleavage of glycosidic bond in nanofibre cellulose into glycosyl unit (Nagarajan et al., 2020). As seen

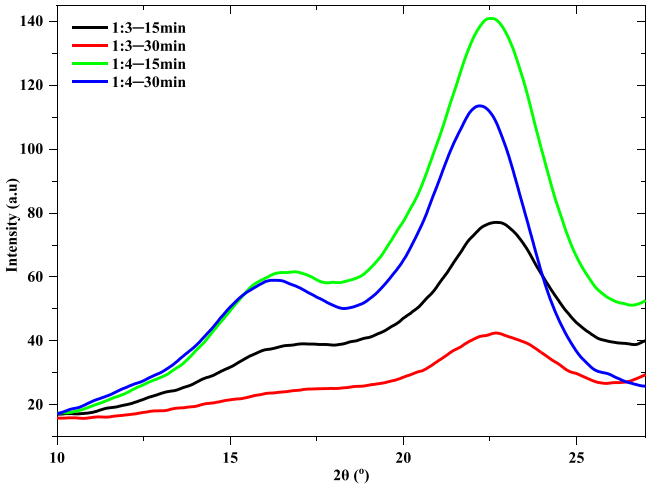

Fig. 8. X-ray diffractogram of ball-milled NFC samples.

Table 3
Crystallinity index of ball milled NFCs.

	I_{AM}	I_{200}	Crystallinity index (%)
1:3—15 min	42.00	103.50	59.42
1:3—30 min	30.00	62.50	52.00
1:4—15 min	70.00	209.50	66.59
1:4—30 min	54.50	153.50	64.50

in Table 4, 1:3—15 min, 1:3—30 min, 1:4—15 min, 1:4—30 min started to decompose at 271.40 ℃, 269.59 ℃, 286.87 ℃ and 276.19 ℃ respectively and the decomposition temperature range of 1:4—15 min relatively shifted to high temperature due to enhancing in crystallinity index (Solikhin et al., 2019). Additionally, high crystallinity index of 1:4—15 min, increase the maximum thermal degradation temperature T_{max}, which is 323.39 ℃ as shown in DTG curve (Shahi et al., 2020). The maximum thermal degradation denotes the thermal stability of NFCs as well. Therefore the crystalline regions of NFC act as barriers for the heat transfer, in order to improve the thermal stability of NFC (Gea et al., 2020). Based on literature, the obtained thermal stability of NFC is comparatively higher than the other ball-milled NFCs, which are obtained from cellulose powder (220 ℃), sugarcane bagasse (229 ℃) and paper waste (140 ℃) (Nagarajan et al., 2019). The decrement of T_{max} for 30 min milled NFC, may be due to breakdown of crystalline region as the high mechanical treatment. This fact, cause difficulty on realignment of crystalline region in orderly manner during lyophilization (Seta et al., 2020). Among the ball-milled nanofibre cellulose, 1:4—30 min and 1:3—30 min displayed highest residue content at 700 ℃, which is 35.37% and 31.72% accordingly. This is anticipated to the presence of non-cellulosic or trace elements during milling (Pakutsah and Aht-Ong, 2020). According to Hernandez-Varela et al. (2020) the extended ball milling time, grinds the PALF nanofibre but the stimulated stress from inside of the vessels, increasing the interaction of fibre-ball milling material which triggering cross-contamination from the wall of container and possibly from milling balls.

4. Conclusion

The proposed work mainly focusses on exploring green protocol for the utilisation of N36 *Ananas comosus* leaves fibre (PALF) to highly potential material. Cellulose nanofibre were successfully isolated from PALF by ball milling with presence of isopropyl alcohol as solvent. Mild thermo-chemical treatment prior to ball milling respond to removal of non-cellulosic component and increase the feasibility of defibrillation of PALF fibre. The effect of IPA and the milling time on nano fibrillation

Table 4
Thermogravimetric degradation summary of PALF nanofibre.

NFC	MS (%)	T_{on} ℃	T_{off} ℃	T_{max} ℃	Residue at 700 ℃ (%)
1:3—15 min	5.85	271.40	321.35	303.25	25.55
1:3—30 min	7.23	269.59	321.07	301.48	31.72
1:4—15 min	13.4	286.87	341.06	323.39	12.59
1:4—30 min	9.13	276.19	330.19	311.79	35.37

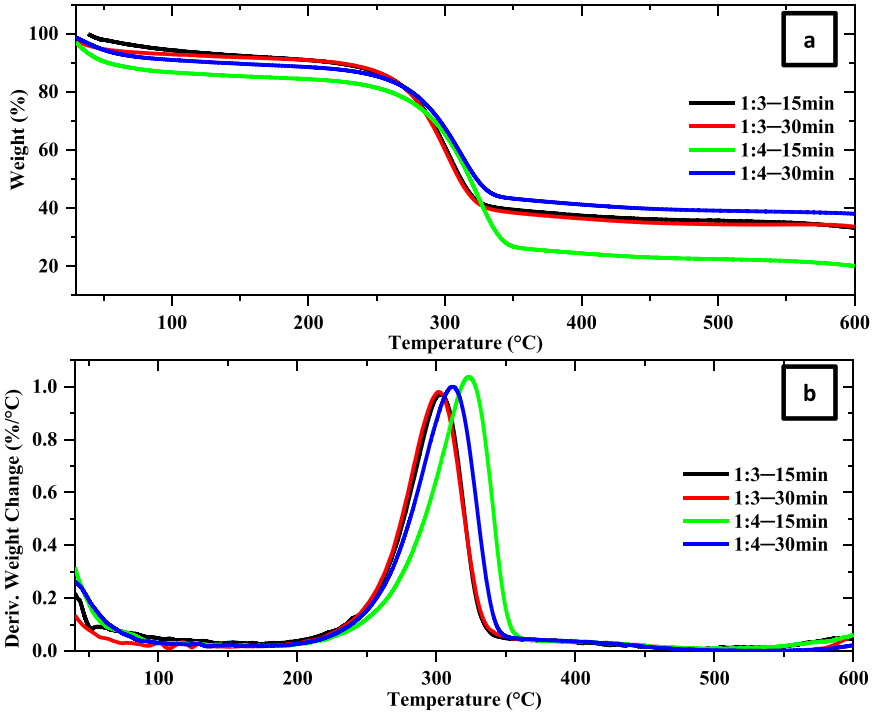

Fig. 9. (a) TGA and (b) DTG curve of milled NFCs.

were analysed through characterisation of NFCs. Comparatively, 1:4—15 min sample express desirable features in the concern of morphology, fibre size, yield, crystallinity, thermal stability, and homogeneity on disintegration of PALF fibre. Highest thermal degradation temperature of 323.39 ℃ and has high crystallinity index of 66.59%, reveal huge prospective on reinforcing in high temperature composite. Moreover, it exhibits excellent surface morphology, stability (low agglomeration), and uniformity in defibrillation with fibre diameter of 25.84 ± 8.30 nm, zeta-potential of − 32.31 ± 2.51 and PDI of 0.103. Hence, addition of IPA gives significant impact on defibrillation by disrupt the intermolecular hydrogen bond, so that less milling time is convenient on production of NFC without causes severe damage on other properties.

CRediT authorship contribution statement

Surenthiran Gnanasekaran: Formal analysis, Investigation, Writing – original draft. **Noor Ida Amalina Ahamad Nordin:** Conceptualization, Supervision, Validation, Writing – review & editing, Funding acquisition. **Saidatul Shima Jamari:** Visualization, Validation, Software, Resources. **Jun Haslinda Shariffuddin:** Resources, Software, Visualization.

Declaration of Competing Interest

The authors declare that they have no known competing financial interests or personal relationships that could have appeared to influence the work reported in this paper.

Acknowledgments

We would like to express our gratitude to Universiti Malaysia Pahang, Malaysia for providing financial support through the research grant PGRS2003129.

References

Ahuja, D., Kumar, L., Kaushik, A., 2021. Thermal stability of starch bionanocomposites films: exploring the role of esterified cellulose nanofibers isolated from crop residue. Carbohydr. Polym. 255, 117466 https://doi.org/10.1016/j.carbpol.2020.117466.

Akinjokun, A.I., Petrik, L.F., Ogunfowokan, A.O., Ajao, J., Ojumu, T.V., 2021. Isolation and characterization of nanocrystalline cellulose from cocoa pod husk (CPH) biomass wastes. Heliyon 7, e06680. https://doi.org/10.1016/j.heliyon.2021.e06680.

Amiralian, N., Annamalai, P.K., Memmott, P., Martin, D.J., 2015. Isolation of cellulose nanofibrils from Triodia pungens via different mechanical methods. Cellulose 22, 2483–2498. https://doi.org/10.1007/s10570-015-0688-x.

Baruah, J., Nath, B.K., Sharma, R., Kumar, S., Deka, R.C., Baruah, D.C., Kalita, E., 2018. Recent trends in the pretreatment of lignocellulosic biomass for value-added products. Front. Energy Res. 6, 1–19. https://doi.org/10.3389/fenrg.2018.00141.

Beyene, D., Chae, M., Dai, J., Danumah, C., Tosto, F., Demesa, A.G., Bressler, D.C., 2018. Characterization of cellulase-treated fibers and resulting cellulose nanocrystals generated through acid hydrolysis. Materials 11. https://doi.org/10.3390/ma11081272.

Boufi, S., Chaker, A., 2016. Easy production of cellulose nanofibrils from corn stalk by a conventional high speed blender. Ind. Crops Prod. 93, 39–47. https://doi.org/10.1016/j.indcrop.2016.05.030.

Cebreiros, F., Seiler, S., Dalli, S.S., Lareo, C., Saddler, J., 2021. Enhancing cellulose nanofibrillation of eucalyptus Kraft pulp by combining enzymatic and mechanical pretreatments. Cellulose 28, 189–206. https://doi.org/10.1007/s10570-020-03531-w.

Czaikoski, A., da Cunha, R.L., Menegalli, F.C., 2020. Rheological behavior of cellulose nanofibers from cassava peel obtained by combination of chemical and physical processes. Carbohydr. Polym. 248, 116744 https://doi.org/10.1016/j.carbpol.2020.116744.

Dilamian, M., Noroozi, B., 2019. A combined homogenization-high intensity ultrasonication process for individualizaion of cellulose micro-nano fibers from rice straw. Cellulose 26, 5831–5849. https://doi.org/10.1007/s10570-019-02469-y.

Ferreira, R.R., Souza, A.G., Nunes, L.L., Shahi, N., Rangari, V.K., Rosa, D., dos, S., 2020. Use of ball mill to prepare nanocellulose from eucalyptus biomass: challenges and process optimization by combined method. Mater. Today Commun. 22, 100755 https://doi.org/10.1016/j.mtcomm.2019.100755.

Fillat, Ú., Wicklein, B., Martín-Sampedro, R., Ibarra, D., Ruiz-Hitzky, E., Valencia, C., Sarrión, A., Castro, E., Eugenio, M.E., 2018. Assessing cellulose nanofiber production from olive tree pruning residue. Carbohydr. Polym. 179, 252–261. https://doi.org/10.1016/j.carbpol.2017.09.072.

Franco, T.S., Potulski, D.C., Viana, L.C., Forville, E., de Andrade, A.S., de Muniz, G.I.B., 2019. Nanocellulose obtained from residues of peach palm extraction (Bactris gasipaes). Carbohydr. Polym. 218, 8–19. https://doi.org/10.1016/j.carbpol.2019.04.035.

Gabriel, T., Wondu, K., Dilebo, J., 2021. Valorization of khat (Catha edulis) waste for the production of cellulose fibers and nanocrystals. PLoS One 16, 1–20. https://doi.org/10.1371/journal.pone.0246794.

Galiwango, E., Abdel Rahman, N.S., Al-Marzouqi, A.H., Abu-Omar, M.M., Khaleel, A.A., 2019. Isolation and characterization of cellulose and α-cellulose from date palm biomass waste. Heliyon 5, e02937. https://doi.org/10.1016/j.heliyon.2019.e02937.

Gea, S., Siregar, A.H., Zaidar, E., Harahap, M., Indrawan, D.P., Perangin-Angin, Y.A., 2020. Isolation and characterisation of cellulose nanofibre and lignin from oil palm empty fruit bunches. Materials 13. https://doi.org/10.3390/ma13102290.

Gnanasekaran, S., Li, Y.Y., Shariffuddin, J.H., Nordin, N.I.A.A., 2020a. Production of cellulose and microcellulose from pineapple leaf fibre by chemical-mechanical treatment. IOP Conf. Ser.: Mater. Sci. Eng. https://doi.org/10.1088/1757-899X/991/1/012055.

Gnanasekaran, S., Muslih, N.S.N., Shariffuddin, J.H., Nordin, N.I.A.A., 2020b. Effect of steam and bleaching treatment on the characteristics of pineapple leaves fibre derived cellulose. Pertanika J. Sci. Technol. 28, 135–148. https://doi.org/10.47836/pjst.28.S2.11.

Gnanasekaran, S., Nordin, N.I.A.A., Hamidi, M.M.B.M., Shariffuddin, J.H., 2021a. Effect of Alkaline treatment on the characteristics of pineapple leaves fibre and PALF / PP biocomposite. J. Mech. Eng. Sci. 15, 8518–8528. https://doi.org/10.15282/jmes.15.4.2021.05.0671.

Gnanasekaran, S., Nordin, N.I.A.A., Jamari, S.S., Shariffuddin, J.H., 2021b. Effect of Steam-Alkaline coupled treatment on N36 cultivar pineapple leave fibre for isolation of cellulose. Mater. Today Proc. 48, 753–760. https://doi.org/10.1016/j.matpr.2021.02.216.

Goh, K.Y., Ching, Y.C., Chuah, C.H., Abdullah, L.C., Liou, N.S., 2016. Individualization of microfibrillated celluloses from oil palm empty fruit bunch: comparative studies between acid hydrolysis and ammonium persulfate oxidation. Cellulose 23, 379–390. https://doi.org/10.1007/s10570-015-0812-y.

Guimaraes, M., Botara, V.R., Novack, K.M., Neto, W.P.F., Mendes, L.M., Tonoli, G.H.D., 2015. Preparation of cellulose nanofibrils from bamboo pulp by mechanical defibrillation for their applications in biodegradable composites. J. Nanosci. Nanotechnol. 15, 6751–6768. https://doi.org/10.1166/jnn.2015.10854.

Han, L., Wang, W., Zhang, R., Dong, H., Liu, J., Kong, L., Hou, H., 2019. Effects of reparation method on the physicochemical properties of cationic nanocellulose and starch nanocomposites. Nanomaterials 9 (12), 1–16. https://doi.org/10.3390/nano9121702.

Hernandez-Varela, J.D., Chanona-Perez, J.J., Villasenor-Altamirano, S.L., Mendoza-Martinez, C., Cervantes Sodi, F., 2020. Changes of crystallinity index and crystallite size in cotton cellulose nanopar by ball milling. 2020 17th International Conference on Electrical Engineering, Computing Science and Automatic Control. CCE 2020. https://doi.org/10.1109/CCE50788.2020.9299162.

Hu, Z., Zhai, R., Li, J., Zhang, Y., Lin, J., 2017. Preparation and characterization of nanofibrillated cellulose from bamboo fiber via ultrasonication assisted by repulsive effect. Int. J. Polym. Sci. 2017. https://doi.org/10.1155/2017/9850814.

Ilyas, R.A., Sapuan, S.M., Ibrahim, R., Abral, H., Ishak, M.R., Zainudin, E.S., Asrofi, M., Atikah, M.S.N., Huzaifah, M.R.M., Radzi, A.M., Azammi, A.M.N., Shaharuzaman, M.A., Nurazzi, N.M., Syafri, E., Sari, N.H., Norrrahim, M.N.F., Jumaidin, R., 2019. Sugar palm (Arenga pinnata (Wurmb.) Merr) cellulosic fibre hierarchy: a comprehensive approach from macro to nano scale. J. Mater. Res. Technol. 8, 2753–2766. https://doi.org/10.1016/j.jmrt.2019.04.011.

Ismail, F., Ali Othman, N.E., Abdul Wahab, N., Abdul Hamid, F., Abdul Aziz, A., 2021. Preparation of microcrystalline cellulose from oil palm empty fruit bunch fibre using steam-assisted acid hydrolysis. J. Adv. Res. Fluid Mech. Therm. Sci. 81, 88–98. https://doi.org/10.37934/arfmts.81.1.8898.

Jahangiri, H., Sönmez, S., Öveçoğlu, M.L., 2016. Influence of milling media on the mechanical alloyed W-0.5 wt% Ti powder alloy. Indian J. Mater. Sci. 2016, 1–6. https://doi.org/10.1155/2016/7981864.

Jaji, K., Man, N., Nawi, N.M., 2018. Factors affecting pineapple market supply in Johor, Malaysia. Int. Food Res. J. 25, 366–375.

Julie Chandra, C.S., George, N., Narayanankutty, S.K., 2016. Isolation and characterization of cellulose nanofibrils from arecanut husk fibre. Carbohydr. Polym. 142, 158–166. https://doi.org/10.1016/j.carbpol.2016.01.015.

Kayes Patoary, M., Zaarour, B., Rashedul Islam, S., Liu, L., 2020. Effects of phosphorylation duration on the jute extracted cellulose nanofibrils using ultrasonication. ChemistrySelect 5, 12750–12758. https://doi.org/10.1002/slct.202003431.

Kian, L.K., Saba, N., Jawaid, M., Sultan, M.T.H., 2019. A review on processing techniques of bast fibers nanocellulose and its polylactic acid (PLA) nanocomposites. Int. J. Biol. Macromol. 121, 1314–1328. https://doi.org/10.1016/j.ijbiomac.2018.09.040.

Lee, S.H., Lee, C.H., Ainun, Z.M.A., Padzil, F.N.M., Lum, W.C., Ahmad, Z., 2020. Improving flame retardancy of pineapple leaf fibers. Green Energy Technol. 123–141. https://doi.org/10.1007/978-981-15-1416-6_7.

Ling, Z., Wang, T., Makarem, M., Santiago Cintrón, M., Cheng, H.N., Kang, X., Bacher, M., Potthast, A., Rosenau, T., King, H., Delhom, C.D., Nam, S., Vincent Edwards, J., Kim, S.H., Xu, F., French, A.D., 2019. Effects of ball milling on the structure of cotton cellulose. Cellulose 26, 305–328. https://doi.org/10.1007/s10570-018-02230-x.

Liu, X., Jiang, Y., Song, X., Qin, C., Wang, S., Li, K., 2019. A bio-mechanical process for cellulose nanofiber production – Towards a greener and energy conservation

solution. Carbohydr. Polym. 208, 191–199. https://doi.org/10.1016/j.carbpol.2018.12.071.
Mahadi, M.B., Rahman, N.A., Manaf, S.F.A., 2015. Isolation of nanocellulose from jatropha waste: an overview. J. Teknol. 76, 37–41. https://doi.org/10.11113/jt.v76.5712.
Mat Zain, N.F., 2014. Preparation and characterization of cellulose and nanocellulose from pomelo (Citrus grandis) Albedo. J. Nutr. Food Sci. 05, 10–13. https://doi.org/10.4172/2155-9600.1000334.
Mazela, B., Perdoch, W., Peplińska, B., Zieliński, M., 2020. Influence of chemical pre-treatments and ultrasonication on the dimensions and appearance of cellulose fibers. Materials 13, 1–14. https://doi.org/10.3390/ma13225274.
Nagarajan, K.J., Balaji, A.N., Ramanujam, N.R., 2019. Extraction of cellulose nanofibers from Cocos nucifera var aurantiaca peduncle by ball milling combined with chemical treatment. Carbohydr. Polym. 212, 312–322. https://doi.org/10.1016/j.carbpol.2019.02.063.
Nagarajan, K.J., Balaji, A.N., Ramanujam, N.R., 2020. Isolation and characterization of cellulose nanocrystals from Saharan Aloe vera cactus fibers. Int. J. Polym. Anal. Charact. 25, 51–64. https://doi.org/10.1080/1023666X.2018.1478366.
Najeeb, M.I., Sultan, M.T.H., Andou, Y., Shah, A.U.M., Eksiler, K., Jawaid, M., Ariffin, A. H., 2020. Characterization of silane treated Malaysian yankee pineapple AC6 leaf fiber (PALF) towards industrial applications. J. Mater. Res. Technol. 9, 3128–3139. https://doi.org/10.1016/j.jmrt.2020.01.058.
Noguchi, Y., Homma, I., Matsubara, Y., 2017. Complete nanofibrillation of cellulose prepared by phosphorylation. Cellulose 24, 1295–1305. https://doi.org/10.1007/s10570-017-1191-3.
Nuruddin, M., Hosur, M., Uddin, M.J., Baah, D., Jeelani, S., 2016. A novel approach for extracting cellulose nanofibers from lignocellulosic biomass by ball milling combined with chemical treatment. J. Appl. Polym. Sci. 133, 1–10. https://doi.org/10.1002/app.42990.
Nurul Atiqah, M.S., Gopakumar, D.A., Owolabi, F.A.T., Pottathara, Y.B., Rizal, S., Sri Aprilia, N.A., Hermawan, D., Paridah, M.T., Thomas, S., Khalil, H.P.S.A., 2019. Extraction of cellulose nanofibers via eco-friendly supercritical carbon dioxide treatment followed by mild acid hydrolysis and the fabrication of cellulose nanopapers. Polymers 11. https://doi.org/10.3390/polym11111813.
Okahisa, Y., Abe, K., Nogi, M., Nakagaito, A.N., Nakatani, T., Yano, H., 2011. Effects of delignification in the production of plant-based cellulose nanofibers for optically transparent nanocomposites. Compos. Sci. Technol. 71, 1342–1347. https://doi.org/10.1016/j.compscitech.2011.05.006.
Pakutsah, K., Aht-Ong, D., 2020. Facile isolation of cellulose nanofibers from water hyacinth using water-based mechanical defibrillation: insights into morphological, physical, and rheological properties. Int. J. Biol. Macromol. 145, 64–76. https://doi.org/10.1016/j.ijbiomac.2019.12.172.
Pereira, P.H.F., Ornaghi, H.L., Arantes, V., Cioffi, M.O.H., 2021. Effect of chemical treatment of pineapple crown fiber in the production, chemical composition, crystalline structure, thermal stability and thermal degradation kinetic properties of cellulosic materials. Carbohydr. Res. 499. https://doi.org/10.1016/j.carres.2020.108227.
Phanthong, P., Karnjanakom, S., Reubroycharoen, P., Hao, X., Abudula, A., Guan, G., 2017. A facile one-step way for extraction of nanocellulose with high yield by ball milling with ionic liquid. Cellulose 24, 2083–2093. https://doi.org/10.1007/s10570-017-1238-5.
Prado, K.S., Spinacé, M.A.S., 2019. Isolation and characterization of cellulose nanocrystals from pineapple crown waste and their potential uses. Int. J. Biol. Macromol. 122, 410–416. https://doi.org/10.1016/j.ijbiomac.2018.10.187.
Radakisnin, R., Majid, M.S.A., Jamir, M.R.M., Jawaid, M., Sultan, M.T.H., Tahir, M.F.M., 2020. Structural, morphological and thermal properties of cellulose nanofibers from napier fiber (Pennisetum purpureum). Materials 13. https://doi.org/10.3390/ma13184125.
Rashid, S., Dutta, H., 2020. Characterization of nanocellulose extracted from short, medium and long grain rice husks. Ind. Crops Prod. 154, 112627 https://doi.org/10.1016/j.indcrop.2020.112627.
Sai Prasanna, N., Mitra, J., 2020. Isolation and characterization of cellulose nanocrystals from Cucumis sativus peels. Carbohydr. Polym. 247, 116706 https://doi.org/10.1016/j.carbpol.2020.116706.
Santucci, B.S., Bras, J., Belgacem, M.N., Curvelo, A.A., da, S., Pimenta, M.T.B., 2016. Evaluation of the effects of chemical composition and refining treatments on the properties of nanofibrillated cellulose films from sugarcane bagasse. Ind. Crops Prod. 91, 238–248. https://doi.org/10.1016/j.indcrop.2016.07.017.
Sartika, D., Syamsu, K., Warsiki, E., Fahma, F., Arnata, I.W., 2021. Nanocrystalline cellulose from kapok fiber (Ceiba pentandra) and its reinforcement effect on alginate hydrogel bead. Starch - Stärke 2100033, 2100033. https://doi.org/10.1002/star.202100033.
Saurabh, C.K., Mustapha, A., Masri, M.M., Owolabi, A.F., Syakir, M.I., Dungani, R., Paridah, M.T., Jawaid, M., Abdul Khalil, H.P.S., 2016. Isolation and characterization of cellulose nanofibers from gigantochloa scortechinii as a reinforcement material. J. Nanomater. 2016. https://doi.org/10.1155/2016/4024527.
Seta, F.T., An, X., Liu, L., Zhang, H., Yang, J., Zhang, W., Nie, S., Yao, S., Cao, H., Xu, Q., Bu, Y., Liu, H., 2020. Preparation and characterization of high yield cellulose nanocrystals (CNC) derived from ball mill pretreatment and maleic acid hydrolysis. Carbohydr. Polym. 234, 115942 https://doi.org/10.1016/j.carbpol.2020.115942.
Shahi, N., Min, B., Sapkota, B., Rangari, V.K., 2020. Eco-friendly cellulose nanofiber extraction from sugarcane bagasse and film fabrication. Sustainability 12, 1–15. https://doi.org/10.3390/su12156015.
Sofla, R.K.M., Brown, R.J., Tsuzuki, T., Rainey, T.J., 2016. A comparison of cellulose nanocrystals and cellulose nanofibres extracted from bagasse using acid and ball milling methods. Adv. Nat. Sci. Nanosci. Nanotechnol. 7. https://doi.org/10.1088/2043-6262/7/3/035004.
Solikhin, A., Hadi, Y.S., Massijaya, M.Y., Nikmatin, S., 2019. Production of microfibrillated cellulose by novel continuous steam explosion assisted chemo-mechanical methods and its characterizations. Waste Biomass Valoriz. 10, 275–286. https://doi.org/10.1007/s12649-017-0066-z.
Sun, X., Wu, Q., Lee, S., Qing, Y., Wu, Y., 2016. Cellulose nanofibers as a modifier for rheology, curing and mechanical performance of oil well cement. Sci. Rep. 6, 1–9. https://doi.org/10.1038/srep31654.
Sun, X., Wu, Q., Zhang, X., Ren, S., Lei, T., Li, W., Xu, G., Zhang, Q., 2018. Nanocellulose films with combined cellulose nanofibers and nanocrystals: tailored thermal, optical and mechanical properties. Cellulose 25, 1103–1115. https://doi.org/10.1007/s10570-017-1627-9.
Supian, M.A.F., Amin, K.N.M., Jamari, S.S., Mohamad, S., 2020. Production of cellulose nanofiber (CNF) from empty fruit bunch (EFB) via mechanical method. J. Environ. Chem. Eng. 8, 103024 https://doi.org/10.1016/j.jece.2019.103024.
Todkar, S.S., Patil, S.A., 2019. Review on mechanical properties evaluation of pineapple leaf fibre (PALF) reinforced polymer composites. Compos. Part B Eng. 174, 106927 https://doi.org/10.1016/j.compositesb.2019.106927.
Wang, J., Xu, J., Zhu, S., Wu, Q., Li, Jinpeng, Gao, Y., Wang, B., Li, Jun, Gao, W., Zeng, J., Chen, K., 2021. Preparation of nanocellulose in high yield via chemi-mechanical synergy. Carbohydr. Polym. 251, 117094 https://doi.org/10.1016/j.carbpol.2020.117094.
Wu, C., McClements, D.J., He, M., Huang, Y., Zhu, H., Jiang, L., Teng, F., Li, Y., 2021. Okara nanocellulose fabricated using combined chemical and mechanical treatments: structure and properties. J. Mol. Liq. 335, 116231 https://doi.org/10.1016/j.molliq.2021.116231.
Xie, H., Du, H., Yang, X., Si, C., 2018. Recent strategies in preparation of cellulose nanocrystals and cellulose nanofibrils derived from raw cellulose materials. Int. J. Polym. Sci. 2018. https://doi.org/10.1155/2018/7923068.
Yang, M., Zhang, X., Guan, S., Dou, Y., Gao, X., 2020a. Preparation of lignin containing cellulose nanofibers and its application in PVA nanocomposite films. Int. J. Biol. Macromol. 158, 1259–1267. https://doi.org/10.1016/j.ijbiomac.2020.05.044.
Yang, X., Reid, M.S., Olsén, P., Berglund, L.A., 2020b. Eco-friendly cellulose nanofibrils designed by nature: effects from preserving native state. ACS Nano 14, 724–735. https://doi.org/10.1021/acsnano.9b07659.
Zhang, L., Tsuzuki, T., Wang, X., 2015. Preparation of cellulose nanofiber from softwood pulp by ball milling. Cellulose 22, 1729–1741. https://doi.org/10.1007/s10570-015-0582-6.
Zheng, Y., Fu, Z., Li, D., Wu, M., 2018. Effects of ball milling processes on the microstructure and rheological properties of microcrystalline cellulose as a sustainable polymer additive. Materials 11, 1–13. https://doi.org/10.3390/ma11071057.